Particle-Size Distribution Effects in Batch Adsorption

Giorgio Carta and Antonio Ubiera
Dept. of Chemical Engineering, University of Virginia, Charlottesville, VA 22903

Mathematical models for pore-diffusion-controlled batch adsorption that take an arbitrary distribution of particle sizes into account are developed and solved for two extreme cases: the linear isotherm case and the irreversible isotherm case. Numerical calculations based on these solutions show that the effects of the particle-size distribution (PSD) are significant, even for relatively narrow and symmetrical PSDs. The uptake rate is faster initially and slower as equilibrium is approached than is predicted using the volume-average particle radius. These results are confirmed by comparing model predictions with experimental results obtained for the batch uptake of the protein α-chymotrypsinogen on SP-Sepharose-FF. Although the PSD of this commonly used commercial medium for preparative protein chromatography is fairly narrow, significant effects are observed in both shallow-bed and stirred batch-uptake experiments. As a result, the PSD needs to be taken into account when precise predictions are desired, such as when batch-uptake experiments are used for diffusivity measurements. The PSD also affects the shape of the breakthrough curve in packed beds. The effects are somewhat less pronounced, but still quite significant for the irreversible isotherm case.

Introduction

Mathematical modeling of adsorption processes is typically based on the assumption that the adsorbent particles are uniform in size and properties. When intraparticle diffusion is controlling, a particle radius equal to the volume average of the particle-size distribution (PSD) is assumed. In spite of the fact that many commercial adsorbents have a broad PSD, this assumption is generally thought to lead to a prediction of the packed-bed adsorptive behavior that is sufficiently accurate for many design purposes.

Several authors have developed models accounting explicitly for the effects of a PSD in the case of linear chromatography. Dougharty (1972) and Moharir et al. (1981) have treated linear chromatographic pulses with moment analyses, while Rasmuson (1985) has obtained an analytical solution for the breakthrough curve. Carta and Bauer (1990) have obtained an explicit solution valid for both pulse and step changes in feed concentration with an arbitrary PSD. These studies have shown that the effect of the PSD on the linear chromatographic behavior can be significant when the PSD is broad and highly asymmetrical, although detailed numerical calculations by Lin and Ma (1990) have shown that these effects have a smaller impact when other factors, such as the nonlinearity of the isotherm, lead to peak tailing.

Significant effects of the PSD can also exist in batch adsorption. While an average particle size can again be used with accuracy typically sufficient for design, when greater accuracy is required, the PSD needs to be taken into account. This can be especially important when batch-absorption data are used for the determination of an effective diffusivity by fitting transient adsorption data with a mass-transfer model. Ruthven and Loughlin (1971) have addressed the effects of crystallite size distribution on diffusion measurements for gas adsorption in molecular sieves. They considered the case of batch adsorption with a constant adsorbate concentration at the surface of the crystallites and obtained an analytical solution for the case of a normally distributed PSD. Although the early portion of the uptake curve was shown to be only slightly dependent on the PSD, significant deviations were observed as equilibrium was approached. As noted by these authors, since it is difficult in practice to determine the initial portion

Correspondence concerning this article should be addressed to G. Carta.

of the uptake curve with high experimental accuracy, fitting over the entire range of the uptake curve is generally desirable. As a result, accounting for the PSD may be needed for the analysis of such data. Batch-uptake rate measurements are also used extensively in liquid-phase adsorption in many areas of application. An example is the case of protein adsorption in chromatography media, whose rate is typically limited by intraparticle diffusion. Many authors (for example, Skidmore et al., 1990; Bloomingburg and Carta, 1994; Yoshida et al., 1994; Tonga et al., 1994; Weaver and Carta, 1996; Chang and Lenhoff, 1998; Garke et al., 1999; Hunter and Carta, 2000; Wesselingh and Bosma, 2001; Chen et al., 2002) have used batch-adsorption rate measurements to determine effective diffusivities of proteins in commercial media. Although monodispersed particles are sometimes used, for economic reasons commercial samples with a distributed PSD are often used in practice. Thus, the extent to which the PSD affects the results needs to be determined.

In this work, we have obtained solutions for batch adsorption accounting for the PSD in the general case of uptake from a finite bath. Two extreme cases are considered—adsorption with a linear isotherm and adsorption with an irreversible isotherm—bracketing the range of possibilities. Both symmetrical and asymmetrical PSDs are considered, as is the PSD of a commercial adsorbent for protein chromatography. The effects of the PSD on the uptake curve are shown to be significant even for moderately dispersed and symmetrical PSDs, suggesting that, in general, these effects need to be taken into account when using batch-uptake data for diffusivity determinations. An experimental system is also discussed as an example of the application of the equations developed in this work.

Theoretical Development

We consider the case of transient adsorption in a closed vessel containing a volume V_p of adsorbent particles and a fluid volume V. Since, in practice, the PSD is expressed as a discrete distribution derived from sieving or obtained from a particle-size analysis instrument, we consider an arbitrary discrete PSD where f_j is the volume fraction of particles of radius r_{pj}. The mean particle size and the standard deviation of the PSD are given by

$$\bar{r}_p = \sum_{j=1}^{M} f_j r_{pj} \tag{1}$$

$$\sigma_p = \sqrt{\sum_{j=1}^{M} f_j \left(r_{pj} - \bar{r}_p\right)^2} \tag{2}$$

where M is the number of particle fractions. It should be noted that normally distributed PSDs are not always found in practice. We further assume that pore diffusion is the dominant transport mechanism, that the adsorption capacity is high compared to the fluid-phase adsorbate concentration, and that local equilibrium exists between the pore fluid and the adsorbed phase at each point within the particles. With these assumptions, material balances yield the following equations and boundary conditions

For each particle j = 1,M

$$\frac{\partial q_j}{\partial t} = \frac{D_e}{r^2}\frac{\partial}{\partial r}\left(r^2\frac{\partial c_j}{\partial r}\right) \tag{3}$$

$$r = 0:\ \frac{\partial c_j}{\partial r} = \frac{\partial q_j}{\partial r} = 0 \tag{3a}$$

$$r = r_{pj}:\ c_j = C \tag{3b}$$

$$t = 0:\ c_j = q_j = 0 \tag{3c}$$

For the fluid phase

$$\frac{dC}{dt} = -3\frac{V_p D_e}{V}\sum_{j=1}^{M}\left[\frac{f_j}{r_{pj}}\left(\frac{\partial c_j}{\partial r}\right)_{r=r_{pj}}\right] = -\frac{V_p}{V}\frac{d\bar{\bar{q}}}{dt} \tag{4}$$

$$t = 0:\ C = C_0 \tag{4a}$$

From Eqs. 4 and 4a, we obtain

$$V(C_0 - C) = V_p\bar{\bar{q}} \tag{5}$$

where

$$\bar{\bar{q}} = \sum_{j=1}^{M} f_j\bar{q}_j = \sum_{j=1}^{M}\left[f_j\frac{3}{r_{pj}^3}\int_0^{r_{pj}} q_j r^2 dr\right] \tag{6}$$

is the concentration in the particles averaged over all particle sizes.

Linear isotherm case

For the linear isotherm case ($q_j = Kc_j$) Eqs. 3 and 4 can be written in dimensionless form as follows

$$\phi_j^2\frac{\partial Y_j}{\partial\tau} = \frac{1}{\rho_j^2}\frac{\partial}{\partial\rho_j}\left(\rho_j^2\frac{\partial Y_j}{\partial\rho_j}\right) \tag{7}$$

$$\rho_j = 0:\ \frac{\partial Y_j}{\partial\rho_j} = 0 \tag{7a}$$

$$\rho_j = 1:\ Y_j = X \tag{7b}$$

$$\tau = 0:\ Y_j = 0 \tag{7c}$$

$$\frac{dX}{d\tau} = -\frac{3\Lambda}{1-\Lambda}\sum_{j=1}^{M}\left[\frac{f_j}{\phi_j^2}\left(\frac{\partial Y_j}{\partial\rho_j}\right)_{\rho_j=1}\right] \tag{8}$$

$$\tau = 0:\ X = 1 \tag{8a}$$

where

$$X = \frac{C}{C_0} \tag{9}$$

$$Y_j = \frac{q_j}{KC_0} \tag{10}$$

$$\rho_j = \frac{r}{r_{pj}} \tag{11}$$

$$\tau = \frac{D_e t}{K \bar{r}_p^2} \tag{12}$$

$$\phi_j = \frac{r_{pj}}{\bar{r}_p} \tag{13}$$

$$\Lambda = \frac{V_p K / V}{1 + V_p K / V} \tag{14}$$

where Λ is the fraction of adsorbate in the particles when equilibrium is attained. It should be noted that these equations are also formally equivalent to the case of surface or solid-phase diffusion, by taking the surface diffusivity $D_s = D_e/K$ (LeVan et al., 1997).

An analytical solution of these equations can be obtained by applying the Laplace transform. Equations 7–8 are transformed into

$$s\phi_j^2 \tilde{Y}_j = \frac{1}{\rho_j^2} \frac{d}{d\rho_j} \left(\rho_j^2 \frac{d\tilde{Y}_j}{d\rho_j} \right) \tag{15}$$

$$\rho_j = 0: \ \frac{d\tilde{Y}_j}{d\rho_j} = 0 \tag{15a}$$

$$\rho_j = 1: \ \tilde{Y}_j = \tilde{X} \tag{15b}$$

$$s\tilde{X} - 1 = -\frac{3\Lambda}{1-\Lambda} \sum_{j=1}^{M} \left[\frac{f_j}{\phi_j^2} \left(\frac{d\tilde{Y}_j}{d\rho_j} \right)_{\rho_j = 1} \right] \tag{16}$$

Integrating Eq. 15 and substituting the result in Eq. 16 yields

$$\tilde{X} = \frac{1}{s + \dfrac{3\Lambda}{1-\Lambda} \displaystyle\sum_{j=1}^{M} \left\{ \frac{f_j}{\phi_j^2} \left[\phi_j \sqrt{s} \coth\left(\phi_j \sqrt{s} \right) - 1 \right] \right\}} \tag{17}$$

The time-domain solution is obtained by applying the residue theorem to the general inversion integral (Wylie, 1961). Equation 17 has poles at $s = 0$ and $s = -b_k^2$, where the b_k are the roots of the equation

$$b_k \sum_{j=1}^{M} \left[\frac{f_j}{\phi_j} \cot\left(\phi_j b_k \right) \right] = \frac{1-\Lambda}{3\Lambda} \left[b_k^2 + \frac{3\Lambda}{1-\Lambda} \sum_{j=1}^{M} \left(\frac{f_j}{\phi_j^2} \right) \right] \tag{18}$$

From the residue theorem we thus obtain

$$X = 1 - \Lambda + 6 \frac{1-\Lambda}{\Lambda} \times \sum_{k=1}^{\infty} \frac{\exp\left(-b_k^2 \tau \right)}{3\dfrac{1-\Lambda}{\Lambda} - \dfrac{9}{b_k^2} \displaystyle\sum_{j=1}^{M} \left(\frac{f_j}{\phi_j^2} \right) + 9 \sum_{j=1}^{M} \left[\frac{f_j}{\sin^2\left(\phi_j b_k \right)} \right]} \tag{19}$$

and

$$F = 1 - 6 \frac{1-\Lambda}{\Lambda^2} \times \sum_{k=1}^{\infty} \frac{\exp\left(-b_k^2 \tau \right)}{3\dfrac{1-\Lambda}{\Lambda} - \dfrac{9}{b_k^2} \displaystyle\sum_{j=1}^{M} \left(\frac{f_j}{\phi_j^2} \right) + 9 \sum_{j=1}^{M} \left[\frac{f_j}{\sin^2\left(\phi_j b_k \right)} \right]} \tag{20}$$

where $F = (1 - X)/\Lambda$ is the fractional approach to equilibrium. It can be verified that for an infinite fluid volume ($\Lambda \to 0$), Eq. 20 reduces to

$$F = 1 - \frac{6}{\pi^2} \sum_{k=1}^{\infty} \left\{ \frac{1}{k^2} \sum_{j=1}^{M} \left[f_j \exp\left(-k \frac{\pi^2}{\phi_j^2} \tau \right) \right] \right\} \tag{21}$$

which is analogous to the result of Ruthven and Loughlin (1971). Conversely, if the adsorbent particles are uniform, Eq. 20 reduces to the well-known expression (Ruthven, 1984)

$$F = 1 - 6 \frac{1-\Lambda}{\Lambda^2} \sum_{k=1}^{\infty} \frac{\exp\left(-p_k^2 \tau \right)}{\dfrac{9}{\Lambda} + \left(\dfrac{1}{\Lambda} - 1 \right)^2 p_k^2} \tag{22}$$

where the p_k are the roots of

$$p_k \cot p_k = \frac{1-\Lambda}{3\Lambda} \left(p_k^2 + \frac{3\Lambda}{1-\Lambda} \right) \tag{23}$$

Irreversible isotherm case

In the case of an irreversible or "rectangular" isotherm ($q = q_m H(c)$), a sharp adsorption front separating a clean core from a completely saturated layer is quickly established in each particle. The position of the front, r_{sj}, is given by the following equation and boundary condition (Ruthven, 1984)

$$q_m r_{sj}^2 \frac{dr_{sj}}{dt} = \frac{D_e C}{\dfrac{1}{r_{pj}} - \dfrac{1}{r_{sj}}} \tag{24}$$

$$t = 0: \ r_{sj} = r_{pj} \tag{24a}$$

while the amount adsorbed in each particle is given by

$$\frac{\bar{q}_j}{q_m} = 1 - \left(\frac{r_{sj}}{r_{pj}} \right)^3 \tag{25}$$

In dimensionless form, these equations can be written as

$$\frac{d\psi_j}{d\tau} = \frac{6}{\phi_j^2} X \tag{26}$$

$$\tau = 0: \ \psi_j = 0 \tag{26a}$$

where

$$\psi_j = 2\rho_{sj}^3 - 3\rho_{sj}^2 + 1 \tag{27}$$

$$\tau = \frac{D_e t}{\bar{r}_p^2}\frac{C_0}{q_m} \tag{28}$$

The fluid-phase concentration is given by

$$X = 1 - \lambda \sum_{j=1}^{M} \left[f_j \left(1 - \rho_{sj}^3\right)\right] \tag{29}$$

where $\lambda = V_p q_m / V C_0$. Equation 26 actually corresponds to a system of M differential equations. However, from this equation it follows that

$$d\psi_j = \left(\frac{r_{pM}}{r_{pj}}\right)^2 d\psi_M \tag{30}$$

or, integrating, that

$$2\rho_{sj}^3 - 3\rho_{sj}^2 + 1 = \left(\frac{r_{pM}}{r_{pj}}\right)^2 \psi_M \tag{31}$$

where we have chosen M to refer to the largest particle in the PSD. Solving the cubic Eq. 31 for ρ_{sj} yields

$$\rho_{sj} = \frac{1}{2} + \cos\left\{\frac{\pi}{3} + \frac{1}{3}\cos^{-1}\left[1 - 2\left(\frac{r_{pM}}{r_{pj}}\right)^2 \psi_M\right]\right\} \tag{32}$$

Thus, the problem reduces to the solution of the single differential equation

$$\frac{d\psi_M}{d\tau} = \frac{6}{\phi_M^2}\left\{1 - \lambda \sum_{j=1}^{M} f_j \left\{1 - \left\{\frac{1}{2} + \cos\left\{\frac{\pi}{3} + \frac{1}{3} \times \cos^{-1}\left[1 - 2\left(\frac{r_{pM}}{r_{pj}}\right)^2 \psi_M\right]\right\}\right\}^3\right\}\right\} \tag{33}$$

$$\tau = 0: \ \psi_M = 0 \tag{33a}$$

which is easily integrated numerically with the condition that $\rho_{sj} \geq 0$ or $(r_{pM}/r_{pj})^2 \psi_M \leq 1$. Once ψ_M is known as a function of time, X and $\bar{\bar{q}}$ are calculated from Eqs. 32, 29, and 6.

The limiting case for an infinite fluid volume ($\lambda \to 0$) is

$$\frac{\bar{\bar{q}}}{q_m} = \sum_{k=1}^{M} f_j \left\{1 - \left\{\frac{1}{2} + \cos\left\{\frac{\pi}{3} + \frac{1}{3}\cos^{-1}\left[1 - \frac{12}{\phi_j^2}\tau\right]\right\}\right\}^3\right\} \tag{34}$$

while the solution for uniform particles is derived by Teo and Ruthven (1986), and is given in LeVan et al. (1997).

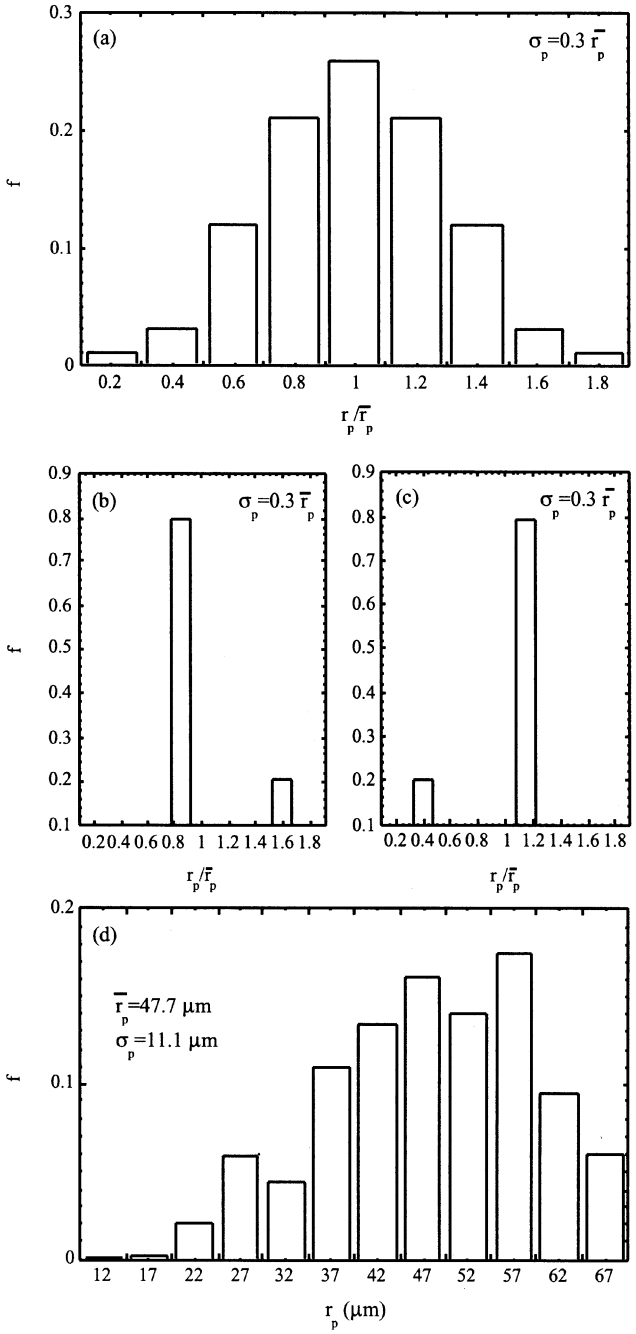

Figure 1. Particle-size distributions used in this work.

(a), (b), (c) Fictitious distributions; (d) is the particle-size distribution for the SP-Sepharose-FF sample used in the experimental work.

Computational Results

Numerical calculations were performed for different cases based on the PSDs shown in Figure 1. The first three distributions (Figures 1a–1c) are fictitious, while the fourth (Figure 1d) corresponds to the experimental system discussed later. The first three distributions have the same mean particle size and standard deviation. However, the first (Figure 1a) is symmetrical, while the other two are bimodal and asymmetrical. Figure 1b corresponds to a sample of small

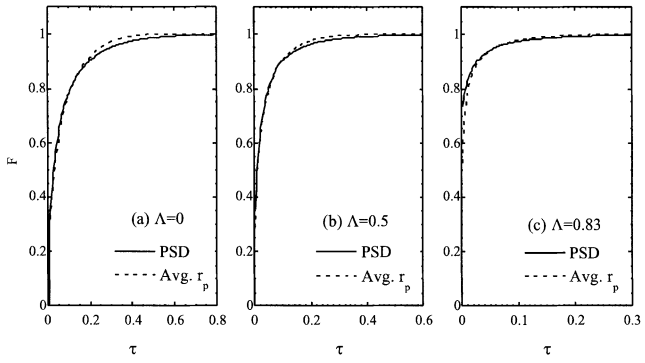

Figure 2. Batch-uptake curves for the linear isotherm case predicted using the PSD in Figure 1a and the average particle radius.

(a) Infinite bath; (b) finite bath with $\Lambda = 0.5$; (c) finite bath with $\Lambda = 0.83$.

particles containing a small percentage of large particles, while Figure 1c corresponds to a sample with a small fraction of "fines." For the linear isotherm case, the roots of Eq. 18 are located within the intervals $\pi k/\phi_j < b_k < \pi(k+1)/\phi_j$ and were obtained numerically using the "goal seek" function in Microsoft Excel. The first 20 roots were used in the calculations. For the irreversible isotherm case, Eq. 33 was solved numerically using Euler's method. Results are shown in Figure 2 for the linear isotherm case and in Figures 3 and 4 for the irreversible isotherm case for different values of Λ (or λ). Values of Λ (or λ) equal to zero correspond to a constant fluid-phase concentration ("infinite bath").

As shown in Figure 2 for the linear isotherm case, the uptake rate predicted taking into account the PSD is faster initially and slower later as compared to predictions based on the volume-average particle radius. The two solutions cross at a time that depends on the value of Λ, and the differences between the two solutions are greater when $\Lambda = 0$. In the case of the irreversible isotherm shown in Figure 3, the differences between the PSD solution and the solution based on the average particle radius are more pronounced. In all three cases, the uptake rate is faster initially and slower later for

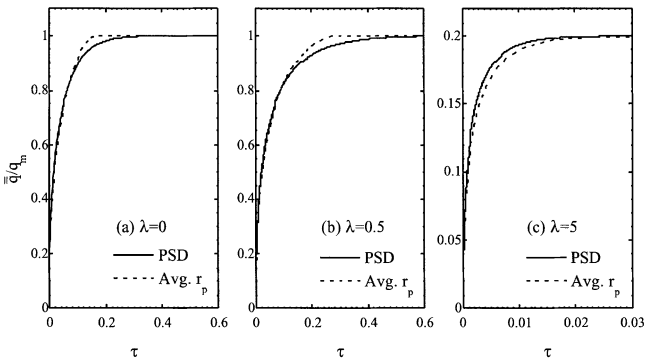

Figure 3. Batch-uptake curves for the irreversible isotherm case predicted using the PSD in Figure 1a and the average particle radius.

(a) Infinite bath; (b) finite bath with $\lambda = 0.5$; (c) finite bath with $\lambda = 5$.

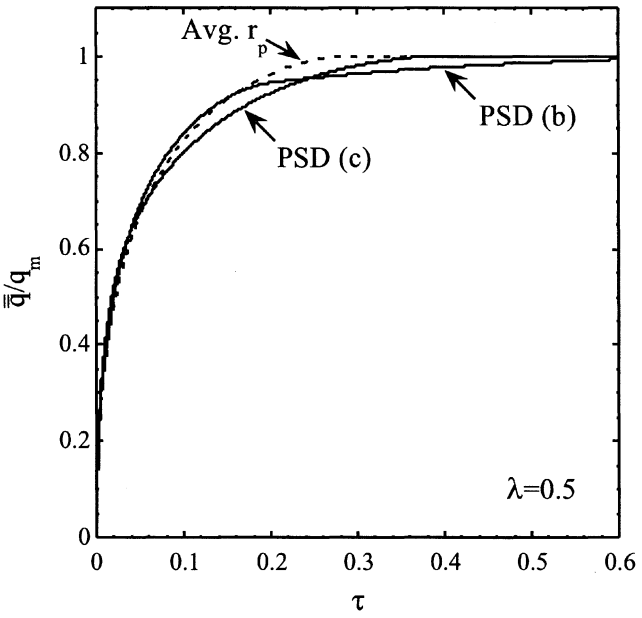

Figure 4. Batch-uptake curves for the irreversible isotherm case predicted using the PSD in Figures 1a, 1b, and the average particle radius in a finite bath with $\lambda = 0.5$.

the PSD case. However, as equilibrium is approached, very large differences in rate are observed. This occurs because, after a time, the smaller particles are completely saturated and no longer contribute to the overall uptake rate. This was not the case for the linear isotherm (or when surface or solid-phase diffusion is dominant), where all particles, large or small, approach saturation in an infinite time. An interesting effect is seen in Figure 3c for $\lambda = 5$, which corresponds to a case where the amount of adsorbate initially in the fluid phase is only 20% of the amount required to completely saturate the particles. In this case, adsorption stops when $\bar{\bar{q}}/q_m = 0.2$. We see that the uptake curve predicted accounting for the PSD always lies above the curve based on the average particle size. This means that, in practice, neglecting the PSD effect would give the impression of a faster uptake rate at higher values of λ (that is, higher V_p or lower C_0).

Figure 4 shows calculated uptake curves for the irreversible isotherm case for the PSDs shown in Figures 1b and 1c. The crossover of the solution accounting for the PSD and the one based on the average particle radius is different for the two cases. The departure is perhaps more dramatic when the adsorbent sample contains a small fraction of large particles (PSD in Figure 1b). In this case, following a fairly rapid initial rate, the uptake slows down dramatically when the small particles are completely saturated.

Comparison with Experiments

The experimental system considered in this work is the adsorption of the protein α-chymotrypsinogen (αCHY) on SP-Sepharose-FF. αCHY has a molecular mass $M_r \sim 26{,}000$, a pI ~ 9.5 (Righetti and Caravaggio, 1976), and a solution diffusivity of 9.3×10^{-7} cm^2/s (Tyn and Gusek, 1990). It was obtained from Sigma Chemical Co. (St. Louis, MO). SP-

Sepharose-FF is a very common commercial cation exchanger, based on a porous agarose matrix. It was obtained from Amersham Biosciences (Uppsala, Sweden). The adsorption of cationic proteins on this material is very favorable at low ionic strengths. As demonstrated by Ljunglöf and Thommes (1998) and Dziennik et al. (2003) by means of confocal fluorescence microscopy of labeled proteins, a sharp adsorption front is established in the particles, consistent with a pore-diffusion mechanism and irreversible binding.

The particle-size distribution of the SP-Sepharose-FF sample used in this work was determined from microphotographs at 100× magnification and is shown in Figure 1d. The particles are essentially perfect spheres, so that particle size is readily determined. The distribution is consistent with that previously reported by Bloomingburg and Carta (1994), although the average particle radius is somewhat larger ($\bar{r}_p$ = 47.7 μm). Experiments were performed in a pH 6.5 sodium phosphate buffer at an ionic strength of 20 mM. The αCHY concentration in solution was determined spectrophotometrically at 280 nm. Particle volumes were determined using the weight of dry media and the particle density (g dry weight/mL of hydrated particle) obtained picnometrically.

Figure 5 shows the uptake equilibrium isotherm for αCHY. This was obtained by allowing samples of SP-Sepharose-FF to equilibrate with solution volumes containing different concentrations of αCHY for 8–24 h. The amount adsorbed at equilibrium (there was no difference between the 8 h and 24 h measurements) was determined using a material balance from the residual solution concentration of αCHY. As seen in Figure 5, the isotherm is very favorable and the solid line shows the Langmuir fit of these data. However, given the scatter and the limited accuracy in the determination of αCHY at low concentration, the experimental data are not distinguishable from a rectangular isotherm.

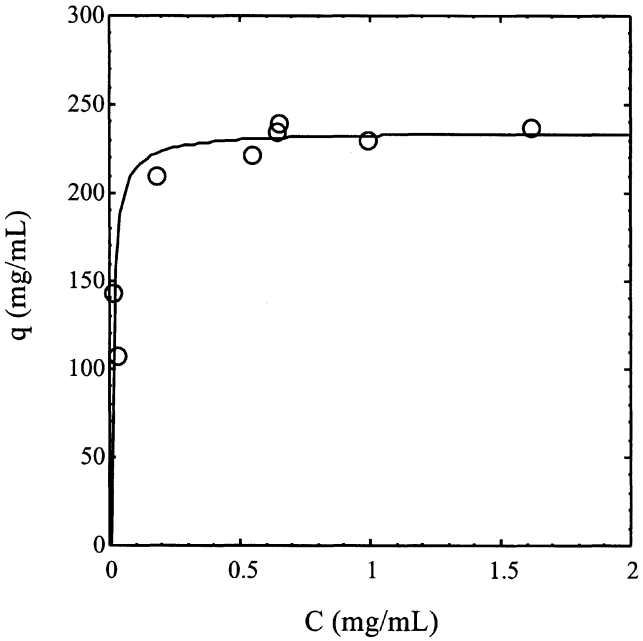

Figure 5. Adsorption isotherm for α-chymotrypsinogen on SP-Sepharose-FF in pH 6.5 sodium phosphate buffer with an ionic strength of 20 mM.

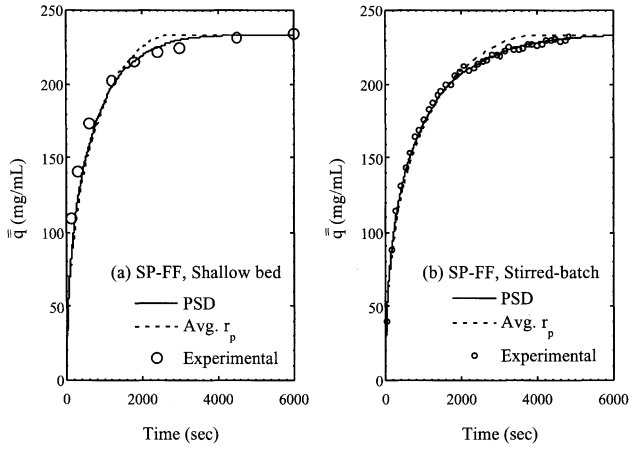

Figure 6. Comparison of experimental and predicted batch-uptake curves for α-chymotrypsinogen on SP-Sepharose-FF in pH 6.5 sodium phosphate buffer with an ionic strength of 20 mM.

(a) Shallow-bed uptake with $C_0 = 1$ mg/mL; (b) stirred batch uptake with $C_0 = 1$ mg/mL, $V_p = 0.16$ mL, $V = 100$ mL. The lines are calculated with $D_e = 3.3 \times 10^{-7}$ cm^2/s using the experimental PSD and the average particle radius.

Transient uptake curves of αCHY on SP-Sepharose-FF are shown in Figure 6 for both a shallow-bed and a stirred-batch experiment. The shallow-bed experiment was conducted in a manner similar to that described by Hunter and Carta (2000). For this experiment a small sample of SP-Sepharose-FF (~5 μL) was placed in a 0.5-cm ID glass chromatographic column fitted with two adjustable plungers (Amersham Biosciences, Model HR 5/5). For an uptake experiment, a solution containing 1 mg/mL αCHY is passed through this column for a certain period of time at a high flow rate (4 mL/min). Excess protein is then quickly removed from the extraparticle voids by feeding the protein-free buffer. This is followed by a salt solution (500 mM NaCl in the buffer) that causes the adsorbed protein to be desorbed. The amount adsorbed during the time of exposure to the protein solution is determined by integrating the salt elution peak as monitored by a chromatographic detector. The salt is then removed by feeding the protein-free buffer and the cycle repeated for a different period of exposure. Since the amount of adsorbent is very small and the mobile phase velocity is very high, adsorption occurs under essentially constant protein concentration in solution, or for conditions approximating an infinite bath. An ÄKTA Explorer liquid chromatography system (Amersham Biosciences) was used for these experiments.

Stirred-batch experiments were conducted as described by Hunter and Carta (2000). In these experiments, a sample of the adsorbent particles (0.16 mL) was suspended in a 100-mL sample of a 1.0-mg/mL αCHY solution in a vessel agitated with a magnetically drived impeller at 300 rpm. The protein concentration in solution was continuously monitored by circulating a stream through a UV detector (Amersham Biosciences, UV-1) at 280 nm, using a Cole-Palmer peristaltic pump. The adsorbed protein concentration was determined from a material balance. For these experimental conditions, $\lambda = 0.37$. Thus, at equilibrium, 37% of the protein was adsorbed.

In Figure 6, the experimental results are compared with the irreversible isotherm model, accounting for the PSD and with the average particle radius using an effective diffusivity $D_e = 3.3\times10^{-7}$ cm^2/s. The latter was determined by data fitting. As seen in Figure 6, it is not possible to obtain a good fit using the average particle size for any value of D_e. In fact, a lower D_e-value would result in an underprediction of the initial uptake rate, while a higher D_e-value would result in an even greater overestimation of the uptake rate for long time periods. On the other hand, by taking into account the experimental PSD, the model provides a considerably more satisfactory fit over the entire range. It should be noted that there is greater scatter in the shallow-bed experimental data, since each data point is a separate measurement. These uncertainties are greater for short times as a result of time lags in the apparatus and, especially, errors in the integration of the salt elution peak.

The value of $D_e = 3.3\times10^{-7}$ cm^2/s merits some discussion. This value is about 35% of the free solution diffusivity of αCHY, which is reasonable for pore diffusion in a high porosity medium like SP-Sepharose-FF. We can also compared this value with the diffusivity determined for lysozyme in SP-Sepharose-FF from confocal fluorescence microscopy experiments by Dziennik et al. (2003). At 20-mM ionic strength, these authors find a diffusivity D_e around 4×10^{-7} cm^2/s. This is consistent with the value obtained for αCHY, considering that lysozyme has a lower molecular mass.

Effects on Breakthrough Curves

A final consideration is the effect of the PSD on the breakthrough curve for a packed bed. Analytical solutions are available for the linear isotherm case (Rasmuson, 1985; Carta and Bauer, 1990). For the irreversible isotherm case, a constant pattern solution is readily derived starting with Eq. 26. In terms of the customary dimensionless variables (LeVan et al., 1997), this equation can be written as

$$\frac{d\psi_M}{dN\tau_1} = \frac{6}{15\phi_M^2}X \tag{34}$$

where

$$N = \frac{15(1-\epsilon)D_eL}{u\bar{r}_p^2} \tag{34a}$$

$$\tau_1 = \frac{ut/L-\epsilon}{(1-\epsilon)q_m/C_0} \tag{34b}$$

For a constant pattern, we have

$$X = \bar{\bar{Y}} = \sum_{j=1}^{M} f_j\left(1-\rho_{sj}^3\right) \tag{35}$$

Thus, combining Eqs. 34 and 35 and integrating we obtain

$$N(\tau_1-1) = \int \frac{15\phi_M^2}{6\sum_{j=1}^{M} f_j\left(1-\rho_{sj}^3\right)}\,d\psi_M + \gamma \tag{36}$$

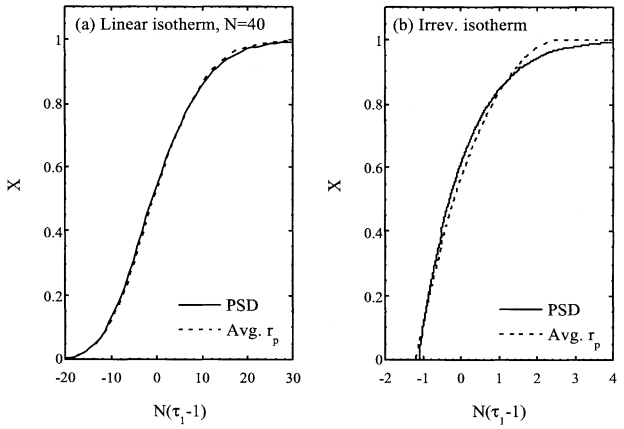

Figure 7. Breakthrough curves predicted using the PSD in Figure 1a and the average particle radius. (a) linear isotherm with $N = 40$; (b) constant pattern solution for irreversible isotherm.

In the general case, this equation, coupled with Eq. 32, has to be integrated numerically with the condition that $\rho_{sj} \geq 0$. The integration constant γ is determined by "centering" the breakthrough curve at $\tau_1 = 1$, so that a material balance is satisfied according to (LeVan et al., 1997)

$$\int_0^1 N(\tau_1-1)\,dX = 0 \tag{37}$$

The limiting case for uniform particles is handled analytically, and the solution is given by Hall et al. (1966).

Figure 7 shows calculated breakthrough curves for the linear isotherm case with $N = 40$, based on the solution of Carta and Bauer (1990), and for the irreversible isotherm case, based on Eq. 36, using both the average particle radius and the PSD of Figure 1a. In both cases, the discrepancy between the solution using the average particle radius and the solution accounting for the PSD seems less pronounced than in batch adsorption. This happens because the average-radius solution tends to underestimate the adsorption rate for short times (corresponding to the downstream portion of the adsorption wave) and overestimate it for long times (corresponding to the upstream portion of the adsorption wave). The breakthrough curve tends to "integrate" these two effects, resulting in a smaller overall difference. However, as seen in Figure 7b, the discrepancy is still substantial for the irreversible isotherm case, especially as the bed approaches saturation.

Conclusions

Mass-transfer models incorporating the PSD of the adsorbent particles were developed and solved for batch adsorption in a finite bath. Numerical calculations based on these models show that the PSD has a significant effect of batch-uptake curves. The effects are more pronounced for broader and more asymmetrical PSDs. In addition they are more pronounced when the isotherm is rectangular than when it is linear. Intermediate isotherm shapes are expected to give intermediate results. Since the error in assuming uniform particles is systematic, it is not possible to accurately fit experi-

mental uptake curves without accounting for the PSD. Experimental results obtained for the adsorption of αCHY on SP-Sepharose-FF at low ionic strength show that the PSD effects have a significant impact on batch-uptake curves, even for the relatively narrow PSD observed for this practical and commonly used protein adsorbent. Of course, in general, other factors, such as a kinetic resistance to adsorption, pore blockage effects, or variations in particle properties, can contribute to the shape of the uptake curve. Nevertheless, the significance of these other potential factors can only be taken into account by first determining the effect of PSD as outlined in this work.

Calculated breakthrough curves for the linear isotherm case show that the impact of the PSD is less pronounced for column calculations when the PSD is only moderately broad and symmetrical, as previously noted by Carta and Bauer (1990). The effect, however, remains significant in the irreversible isotherm case, yielding a breakthrough curve that approaches saturation much more gradually than predicted using the average particle radius.

Acknowledgment

This research was supported by NSF Grant No. CTS-0079334, by the NIH Biotechnology Training Program at the University of Virginia, and by Amersham Biosciences.

Notation

c = adsorbate concentration in pore fluid, mg/mL
C = adsorbate concentration in external fluid, mg/mL
C_0 = initial or feed adsorbate concentration in external fluid, mg/mL
D_e = effective pore diffusivity, cm^2/s
f_j = volume fraction of particles of radius r_{pj}
F = fractional approach to equilibrium
H = unit-step function
K = slope of linear adsorption isotherm
L = bed length, cm
N = number of pore mass-transfer units (Eq. 34a)
q = adsorbed phase concentration, mg/mL
$\bar{q}$ = particle-average adsorbed concentration, mg/mL
$\bar{\bar{q}}$ = sample-average adsorbed concentration, mg/mL
q_m = adsorption capacity, mg/mL
r_p = particle radius, cm
$\bar{r}_p$ = volume-average particle radius, cm
r_s = radial position of adsorption front in particle, cm
t = time, s
u = superficial velocity, cm/s
V = fluid-phase volume, mL
V_p = adsorbent volume, mL
X = dimensionless fluid-phase concentration
Y = dimensionless adsorbed phase concentration

Greek letters

ϵ = bed void fraction
ϕ_j = dimensionless particle radius
λ = capacity factor ($= V_p q_m / V C_0$)
Λ = fraction of adsorbate adsorbed at equilibrium
ρ = dimensionless radial coordinate
ρ_s = dimensionless position of adsorption front
τ = dimensionless time ($= D_e t / K \bar{r}_p^2$ or $D_e t C_0 / \bar{r}_p^2 q_m$)
τ_1 = scaled dimensionless time (Eq. 34b)

Literature Cited

Bloomingburg, G. F., and G. Carta, "Separation of Protein Mixtures by Continuous Annular Chromatography with Step Elution," *Chem. Eng. J.*, **55**, B19 (1994).
Carta, G., and J. S. Bauer, "Analytic Solution for Chromatography with Nonuniform Sorbent Particles," *AIChE J.*, **36**, 147 (1990).
Chang, C., and A. M. Lenhoff, "Comparison of Protein Adsorption Isotherms and Uptake Rates in Preparative Cation-Exchange Materials," *J. Chromatogr. A*, **827**, 281 (1998).
Chen, W.-D., X.-Y. Dong, and Y. Sun, "Analysis of Diffusion Models for Protein Adsorption to Porous Anion-Exchange Adsorbent," *J. Chromatogr. A*, **962**, 29 (2002).
Dougharty, N. A., "Effect of Adsorbent Particle Size Distribution in Gas-Solid Chromatography," *AIChE J.*, **18**, 657 (1987).
Dziennik, S. R., E. B. Belcher, G. A. Barker, M. J. DeBergalis, S. E. Fernandez, and A. M. Lenhoff, "Nondiffusive Mechanisms Enhance Protein Uptake Rates in Ion Exchange Particles," *Proc. Natl. Acad. Sci. USA*, **100**, 420 (2003).
Garke, G., R. Hartmann, M. Papamichael, W.-D. Deckwer, and F. B. Anspach, "The Influence of Protein Size and Shape on Adsorption Kinetics and Equilibria in Ion-Exchange Chromatography," *Sep. Sci. Technol.*, **34**, 2521 (1999).
Hall, K. R., L. C. Eagleton, A. Acrivos, and T. Vermeulen, "Pore and Solid Diffusion Kinetics in Fixed Bed Adsorption under Constant Pattern Conditions," *Ind. Eng. Chem. Fundam.*, **5**, 212 (1966).
Hunter, A. K., and G. Carta, "Protein Adsorption on Novel Acrylamido-Based Polymeric Ion Exchangers—II. Adsorption Rates and Column Behavior," *J. Chromatogr. A*, **897**, 81 (2000).
LeVan, M. D., G. Carta, and C. M. Yon, "Adsorption and Ion Exchange," *Perry's Chemical Engineers' Handbook*, D. W. Green, ed., 7th ed., sect. 16, McGraw-Hill, New York (1997).
Lin, Y. S., and Y. H. Ma, "Analysis of Liquid Chromatography with Nonuniform Crystallite Particles," *AIChE J.*, **36**, 1569 (1990).
Ljunglöf, A., and R. Hjort, "Confocal Microscopy as a Tool for Studying Protein Adsorption to Chromatography Matrices," *J. Chromatogr. A*, **743**, 75 (1996).
Moharir, A. S., D. N. Sharaf, and D. Kunzru, "Effect of Crystal Size Distribution on Chromatographic Peaks in Molecular Sieve Columns," *Chem. Eng. Commun.*, **11**, 377 (1981).
Rasmuson, A., "The Effects of Particles of Variable Size, Shape, and Properties on the Dynamics of Fixed-Beds," *Chem. Eng. Sci.*, **40**, 621 (1985).
Righetti, P. G., and T. Caravaggio, "Isoelectric Points and Molecular Weights of Proteins: A Table," *J. Chromatogr.*, **127**, 1 (1976).
Ruthven, D. M., *Principles of Adsorption and Adsorption Processes*, Wiley, New York (1984).
Ruthven, D. M., and K. F. Loughlin, "The Effect of Crystallite Shape and Size Distribution on Diffusion Measurements in Molecular Sieves," *Chem. Eng. Sci.*, **26**, 577 (1971).
Skidmore, G. L., B. J. Horstmann, and H. A. Chase, "Modeling Single Component Protein Adsorption to the Cation Exchanger S-Sepharose-FF," *J. Chromatogr.*, **498**, 113 (1990).
Teo, W. K., and D. M. Ruthven, "Adsorption of Water from Aqueous Ethanol Using 3-Å Molecular Sieves," *Ind. Eng. Chem. Process Des. Dev.*, **25**, 17 (1986).
Tonga, A., A. I. Liapis, and D. J. Sieher, "Equilibrium and Kinetic Parameters of the Adsorption of α-Chymotrypsinogen A onto Hydrophobic Porous Adsorbent Particles," *J. Chromatogr. A*, **686**, 21 (1994).
Tyn, M. T., and T. W. Gusek, "Prediction of Diffusion Coefficients of Proteins," *Bioeng. Biotechnol.*, **35**, 327 (1990).
Weaver, L. E., and G. Carta, "Protein Adsorption on Cation Exchangers: Comparison of Macroporous and Gel-Composite Media," *Biotechnol. Progr.*, **12**, 342 (1996).
Wesselingh, J. A., and J. C. Bosma, "Protein Ion Exchange Adsorption Kinetics," *AIChE J.*, **47**, 1571 (2001).
Wylie, C. R., *Advanced Engineering Mathematics*, McGraw-Hill, New York (1961).
Yoshida, H., M. Yoshikawa, and T. Kataoka, "Parallel Transport of BSA by Surface and Pore Diffusion in Strongly Basic Chitosan," *AIChE J.*, **40**, 2034 (1994).

Manuscript received Mar. 5, 2003, and revision received May 12, 2003.